Casimir-Lifshitz force variations across heterogeneous gapped metal surfaces

M. Boström [1,2,*] S. Pal [1] H. R. Gopidi [1] S. Osella [2] A. Gholamhosseinian [3] G. Palasantzas [4] and O. I. Malyi [5,1,†]

[1] *Centre of Excellence ENSEMBLE3 Sp. z o. o., Wolczynska Str. 133, 01-919 Warsaw, Poland*

[2] *Chemical and Biological Systems Simulation Lab, Centre of New Technologies, University of Warsaw, Banacha 2C, 02-097 Warsaw, Poland*

[3] *Department of Physics, Ferdowsi University of Mashhad, Mashad 9177948974, Iran*

[4] *Zernike Institute for Advanced Materials, University of Groningen, Groningen 9747 AG, Netherlands*

[5] *Qingyuan Innovation Laboratory, Quanzhou, 362801, People's Republic of China*

(Received 14 February 2024; revised 18 April 2024; accepted 21 June 2024; published 12 July 2024)

The Casimir-Lifshitz force is calculated between a heterogeneous gapped metal surface and a silica (gold) sphere attached to an atomic force microscope (AFM) cantilever tip. We demonstrate that heterogeneous surface patches with different off-stoichiometry surface properties lead to changes in the predicted distances for a specific force. This can incorrectly be interpreted as occurrences of surface roughness.

DOI: 10.1103/PhysRevB.110.045424

I. INTRODUCTION

With the development of solid-state physics and quantum theory, it becomes clear that the interaction between the closely spaced objects originates from the fluctuation of the electromagnetic field, defining the Casimir interaction [1]. The fundamental physics of this interaction has been developed for a range of simple geometries and is defined by the dielectric properties of the interacting materials [2]. This foundation formed the basis for our understanding of Casimir's effect for real metal surfaces [3–5], repulsive Casimir forces with topological insulators [6], Casimir torque [7], and for cylinders across magnetic fluids [8]. Force measurements have, for instance, been carried out using a torsion pendulum [9,10] and with the help of AFM [11], e.g., in sphere-plate setups. It is widely believed that the dielectric properties of many materials are weakly affected by the environmental conditions, since, under standard conditions, the environmental effect is predominantly limited to the concentration of defects within a specific material [12]. However, with the emergence of electronic structure theory, a new type of materials—gapped metals—has been identified. What makes these materials special is that they exhibit the superposition of both insulating and metallic properties, i.e., having an internal gap and larger free carrier concentration due to the Fermi level residing in the principal conduction (i.e., n-type) or valence band (i.e., p-type). Such a unique electronic structure not only results in unique dielectric properties but also offers a knob that can be used to tune materials properties [13]. Specifically, gapped metals can develop spontaneous off-stoichiometry due to Fermi level instability [14], resulting in the formation of a range of off-stoichiometric compounds, all having different electronic properties. Taking into account that the dielectric properties of any given material are closely related to electronic structure, it becomes clear that such a knob can also be used to tune the Casimir interaction.

Moving from this theoretical framework to practical investigation, AFM becomes the technique of choice when the Casimir interaction plays a dominant role. Consider, for instance, the case of AFM measurements of materials roughness, where the typical materials profile is extracted based on a specific physical model of the interactions involved. In the case of homogeneous samples, such material profiles can be well theoretically motivated. However, for commonly observed heterogeneous samples, different regions of the samples can result in different interactions with the tip. The observed force is highly sensitive to both surface roughness and optical properties at separations less than 100 nm, as reported by Broer *et al.* [15]. Motivated by this, in this paper, we explore the fundamental theory of the Casimir interaction for gapped metal surfaces. Notably, our results clearly demonstrate how a change in stoichiometry can result in changes in the Casimir forces, which can be misinterpreted as a change of roughness when not properly accounting for heterogeneous surface-specific properties.

II. THEORY

To study and model the dielectric properties of the relevant materials, we performed first-principles calculations using the Perdew-Burke-Ernzerhof (PBE) exchange-correlation functional [16] with DFT+U correction for Nb (U = 1.5 eV) *d*-like orbitals as implemented by Dudarev *et al.* [17], available within the Vienna *Ab initio* Simulation Package (VASP) [18–21]. Our analysis focuses on two representatives sets of gapped metals, (i) $Ba_{1-x}Nb_{1-y}O_3$ (with five different compositions) and (ii) $Ca_{6-x}Al_7O_{16}$ (with three different compositions), previously identified to be stable with respect to decomposition into the competing phases [13]. We compute the dielectric properties for each system, considering only the Drude contribution and interband transitions. For the calculations of direct band transitions and plasma frequencies we

*Contact author: mathias.bostrom@ensemble3.eu

†Contact author: oleksandrmalyi@gmail.com

 ©2024 American Physical Society

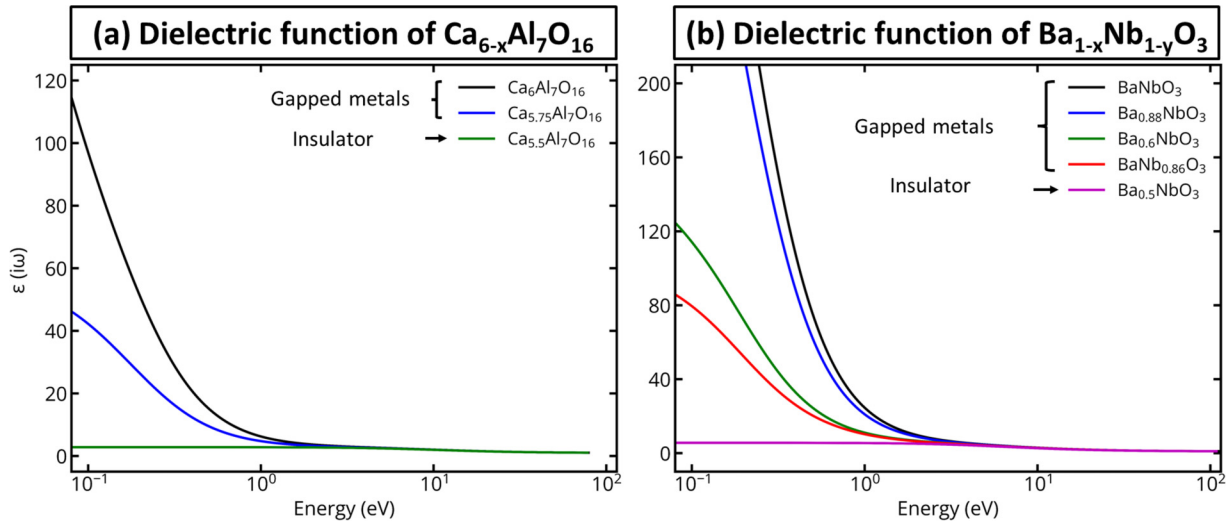

FIG. 1. (a) Dielectric functions for imaginary frequencies from top to bottom for $Ca_6Al_7O_{16}$, $Ca_{5.75}Al_7O_{16}$, and $Ca_{5.5}Al_7O_{16}$. (b) Dielectric functions for imaginary frequencies from top to bottom for $BaNbO_3$, $BaNb_{0.88}O_3$, $Ba_{0.6}NbO_3$, $BaNb_{0.86}O_3$, and $Ba_{0.5}NbO_3$. The results include a superposition of interband transitions and Drude (free electron) contributions [with damping coefficient (Γ) set to 0.2 eV], both calculated using DFT.

introduced a small Lorentzian broadening of 0.01 eV in the Kramers-Kronig transformation [22]. To include the Drude term in the optical properties, we utilize the kram code (which is part of WIEN2k [23,24]), setting the damping coefficient (Γ) to 0.2 eV. Additional details on computational parameters can be found in our previous paper [13].

From the imaginary part (ε_i'' for material i) of the dielectric function, the quantity related to forces can be obtained,

$$\varepsilon_i(i\xi_m) = 1 + \frac{2}{\pi}\int_0^\infty d\omega \frac{\omega\varepsilon''(\omega)}{\omega^2+\xi_m^2},\ i = 1, 2, 3 \qquad (1)$$

where the Matsubara frequency is $\xi_m = 2\pi kTm/\hbar$, and the subscript i indicates the medium. As seen in Fig. 7 below the curves show strong dependence for the dielectric function on off-stoichiometry for $Ba_{1-x}Nb_{1-y}O_3$ and $Ca_{6-x}Al_7O_{16}$ going from a metallic to insulator behavior. This behavior mainly originated from the spontaneous formation of cation vacancies, originating from energy lowering due to the decay of conducting electrons into the acceptor defect states suggesting that the tuning synthesis/environmental conditions allows to stabilize different gapped metals [13]. To use the DFT calculated dielectric functions shown in Fig. 1 for Casimir-Lifshitz interaction, we also develop the parametrization of the average dielectric function for each of the considered compounds using a 13-mode oscillator model [25],

$$\varepsilon(i\xi) = 1 + \sum_j \frac{C_j}{1+(\xi/\omega_j)^2}. \qquad (2)$$

Here, ω_j and C_j represent the characteristic frequencies and the oscillator strength, respectively. The parameters for each gapped metal are provided in Appendix B.

Let $f(d)$ be the force between a gapped metal (medium 1) and a sphere with radius R (medium 3). For $d << R$ the force between a sphere and a planar surface can be deduced from the free energy $\{F(d) = f(d)/[2\pi R]\}$ between two planar surfaces using the so-called proximity force approximation [3]. The sphere is taken to be made of SiO_2 polymorph (with a volume per SiO_2 unit being 68.82 Å^3 with the details in Ref. [25] and including phonon contribution for low frequencies as done by Boström *et al.* [26,27]). The intervening medium 2 may be a diluted gas with $\varepsilon_2(i\xi_m) = 1$. The force can be written as [2,3]

$$\frac{f(d)}{2\pi R} = \frac{k_BT}{2\pi}{\sum_{m=0}^{\infty}}'\int_0^\infty dq\, q \sum_\sigma \ln\left(1 - r_\sigma^{21} r_\sigma^{23} e^{-2\kappa_2 d}\right), \qquad (3)$$

where σ = TE, TM, k_B is Boltzmann's constant, $\hbar$ is Planck's constant, temperature $T = 300$ K, and the prime in the sum above indicates that the first term ($m = 0$) has to be weighted by 1/2. The Fresnel reflection coefficients between surfaces i and j for the transverse magnetic (TM) and transverse electric

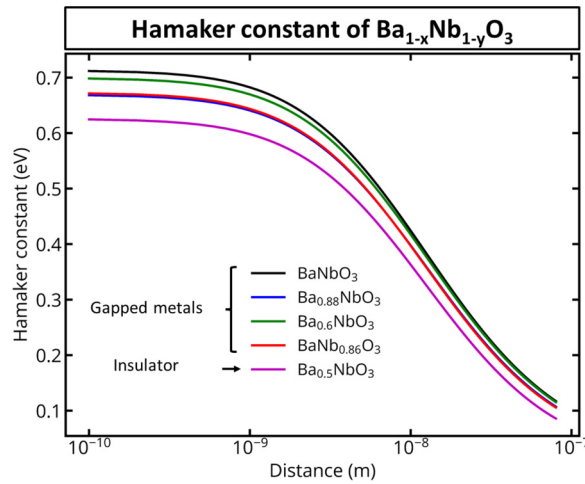

FIG. 2. The retarded Hamaker constant $A^{\rm ret}(d) = -12\pi d^2 \times F(d, T)$ for several material combinations of $Ba_{1-x}Nb_{1-y}O_3$ − air − SiO_2 at temperature $T = 300$ K.

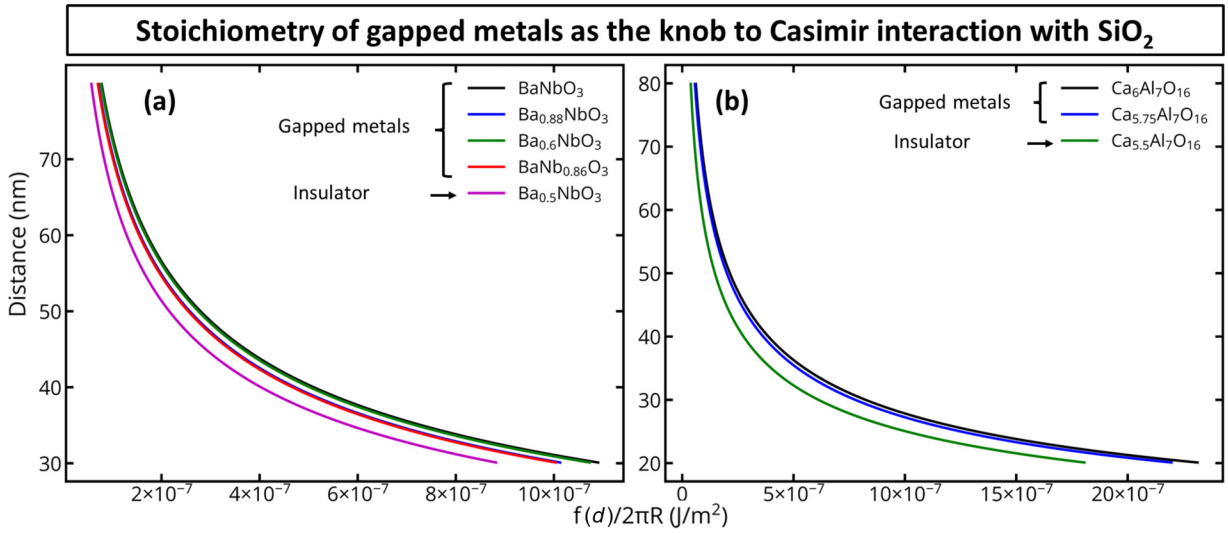

FIG. 3. Distance vs Casimir-Lifshitz force (obtained from proximity force theorem and the expression for the Casimir-Lifshitz free energy) using Eq. (3). In (a) the material combinations are $Ba_{1-x}Nb_{1-y}O_3$-air-SiO_2. In (b), the material combinations are $Ca_{6-x}Al_7O_{16}$-air-SiO_2.

(TE) polarizations are given by

$$r_{\mathrm{TE}}^{ij} = \frac{\kappa_i - \kappa_j}{\kappa_i + \kappa_j}; \quad r_{\mathrm{TM}}^{ij} = \frac{\varepsilon_j \kappa_i - \varepsilon_i \kappa_j}{\varepsilon_j \kappa_i + \varepsilon_i \kappa_j}. \tag{4}$$

Here $\kappa_i = \sqrt{q^2 + \varepsilon_i \xi_m^2 / c^2}$, with $i = 1, 2, 3$ and the Matsubara frequency being $\xi_m = 2\pi k_B T m/\hbar$.

III. RESULTS

A. Silica systems

The relationship between the distance-dependent retarded Hamaker constant $A^{\mathrm{ret}}(d)$ and the corresponding free energy $F(d, T)$ is expressed as $A^{\mathrm{ret}}(d) = -12\pi d^2 \times F(d, T)$. The retarded Hamaker constant between different silica-air-gapped metal systems are illustrated in Fig. 2. This figure illustrates how the interaction is tuned by using various material combinations of $Ba_{1-x}Nb_{1-y}O_3$-air-SiO_2.

TABLE I. The nonretarded Hamaker constant for gapped metal-vapor-SiO_2. With simple manipulation of equations the relative surface correction in the nonretarded limit can be shown equal to $\delta_o = 100 \times (\sqrt{A_s^{NR}/A_o^{NR}} - 1)$ where s correspond to the stoichiometric system (i.e., $BaNbO_3$ and $Ca_6Al_7O_{16}$, respectively) and o are the corresponding off-stoichiometric system. As a comparison, we show the retarded relative surface correction at $d_s = 80$ nm in the right column.

Material	A^{NR} (eV)	δ_o^{NR}	δ_o at $d_s = 80$ nm
$BaNbO_3$	0.71		
$Ba_{0.88}NbO_3$	0.66	3.71%	0.56%
$Ba_{0.6}NbO_3$	0.69	1.43%	3.11%
$BaNb_{0.86}O_3$	0.67	2.94%	3.68%
$Ba_{0.5}NbO_3$	0.63	6.15%	10.8%
$Ca_6Al_7O_{16}$	0.50		
$Ca_{5.75}Al_7O_{16}$	0.48	2.06%	2.59%
$Ca_{5.5}Al_7O_{16}$	0.44	6.6%	16.57%

This figure demonstrates how the interaction strength changes for different material combinations as the distances between particles vary. An attractive interaction can be determined by a positive retarded Hamaker constant, which decreases with increasing distance due to retardation. In the nonretarded (NR) limit of small distances ($d \to 0$) for each material combination, A^{NR} takes a constant value, as listed in Table I. First, let us consider the limit of very small separations when retardation can be neglected. In this case, the Hamaker constant is truly a constant allowing us to calculate a relation between Hamaker constants and the deviations in surface separation (Δd),

$$\frac{A_s(d_s)}{d_s^2} = \frac{A_o(d_o)}{d_o^2} \to \Delta d = d_s - d_o \approx d_o \left(\sqrt{\frac{A_s}{A_o}} - 1 \right), \tag{5}$$

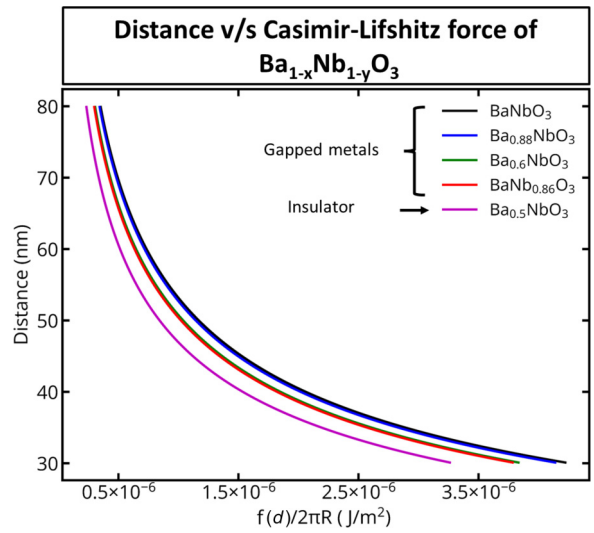

FIG. 4. Distance vs Casimir-Lifshitz force (obtained from proximity force theorem and the expression for the Casimir-Lifshitz free energy). The material combinations are $Ba_{1-x}Nb_{1-y}O_3$-air-Au.

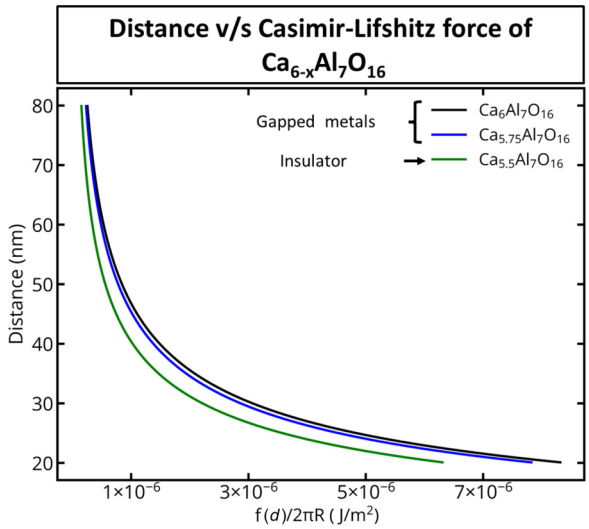

FIG. 5. Distance vs Casimir-Lifshitz force (obtained from proximity force theorem and the expression for the Casimir-Lifshitz free energy). The material combinations are $Ca_{6-x}Al_7O_{16}$-air-Au.

and the percentage correction relative to the stoichiometric surface,

$$\delta_o = (d_s - d_o) \times 100/d_o, \tag{6}$$

$$\delta_o^{NR} = 100 \times \left(\sqrt{A_s^{NR}/A_o^{NR}} - 1\right). \tag{7}$$

The resulting percentage corrections in the nonretarded limit are given in Table I. The question is if these 1–7% distance corrections can give rise to corrections of the same order of magnitude as regular surface roughness.

To this aim, we plot, in a slightly unusual manner, the distance versus force for different $Ba_{1-x}Nb_{1-y}O_3$-air-SiO_2 in Fig. 3(a). Notably, the different distance curves correspond to different spontaneously formed stoichiometric or off-stoichiometric $Ba_{1-x}Nb_{1-y}O_3$ surface patches. Hence, for the same force different surface separations are predicted, corresponding to the tip (sphere) being above different surface patches. To show the generality of the results we present a similar set of curves for $Ca_{6-x}Al_7O_{16}$-air-SiO_2 systems in Fig. 3(b). We observe a clear trend for both systems when going from the most-metallic to the most-insulating surface material.

B. Gold systems

In parallel with calculations for SiO_2 spheres we also consider the case with a gold sphere. The dielectric function for gold was taken from Boström *et al.* [5]. The force curves for gold-air-gapped metals are shown in Figs. 4 and 5. Our proof-of-concept calculations considered a sphere made from either SiO_2 or gold. However, we stress that for an insulating material, one cannot apply any potential to perform electrostatic calibration. Hence, it is not possible to estimate contact potentials allowing for the application of a compensating potential during force measurements to minimize electrostatic contributions. As a result, the forces measured in an experimental setup with insulating materials can, in principle, be contaminated from uncompensated electrostatic contributions due to trapped charges [28]. This is a potential problem that limits any experimental verification of the theory predictions.

C. Inverse design

Our Fig. 6(a) is one main result, and we obtain very similar results when the SiO_2 sphere is replaced with a gold sphere. The results for gold shown in Fig. 6(b) demonstrate the generality of our inverse design approach as a gold-air-gapped metal system can be calibrated for potential electrostatic contributions. The measured force is highly sensitive to both surface roughness and optical properties at separations less

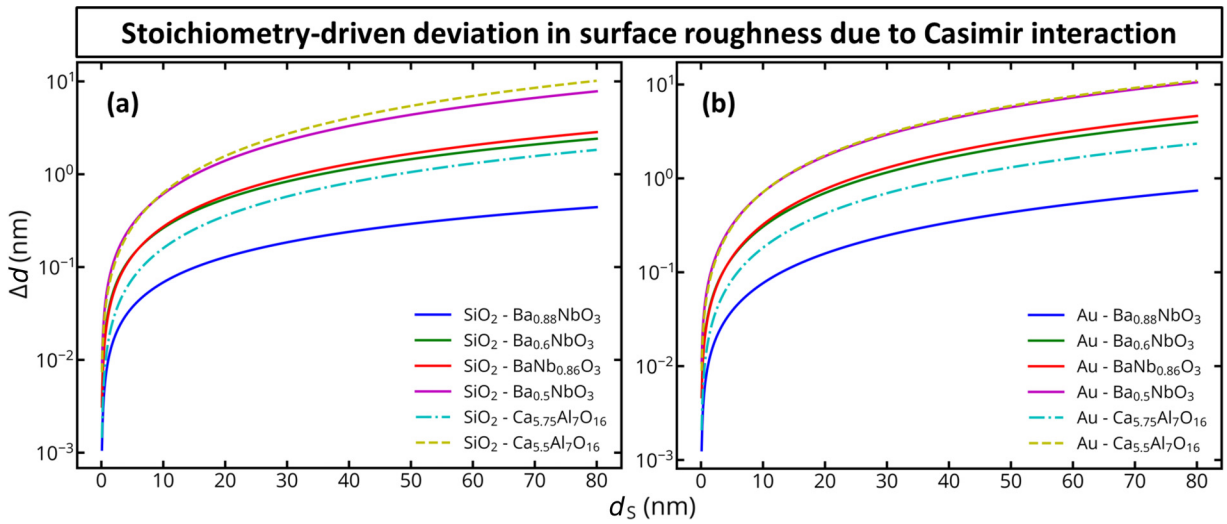

FIG. 6. Here $\Delta d = d_s - d_o$ where s correspond to the stoichiometric system (i.e., $BaNbO_3$ and $Ca_6Al_7O_{16}$, respectively) and o are the corresponding off-stoichiometric system. In this figure, the fitted functions are used to evaluate the value of Δd as a function of d_s. In (a) the sphere is made of silicon and in (b) it is made from gold. While the predicted forces are sensitive to the material of the sphere, we find that the distance variances have similar trends for silica and gold spheres.

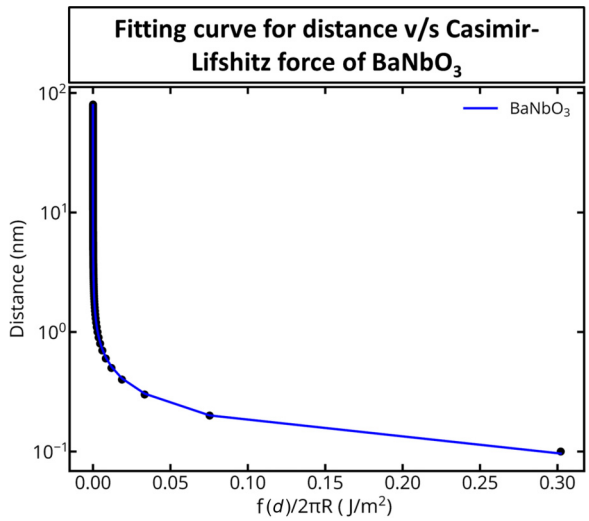

FIG. 7. Fitting curve for distance vs Casimir-Lifshitz force for $BaNbO_3$–air–SiO_2 system.

than 100 nm [15]. The "inverse design" used in the current paper means that we study functions $d(f)$ rather than $f(d)$. The fitting function for d as a function of $x = f/[2\pi R]$ can thus be written as $d = x^{a\,\log(x)}\, x^b\, e^c$ where a, b, and c are unitless fitted parameters given in Appendix A. These fitted functions are used in Figs. 6(a) and 6(b) to evaluate the value of distance variance Δd as a function of d_s, for different material combinations. This allows us to explore some surprisingly large corrections for the predicted surface separations. Notably, when comparing metallic patches with different stoichiometry, the corrections are around 1–4%. However, even larger effects occur when we compare a stoichiometric metallic patch with a patch with an off-stoichiometric insulating state. We predict corrections up to 10–20%. These effects are large enough to impact Casimir force measurements.

IV. CONCLUSIONS

In real-world applications, particularly for those involving heterogeneous surfaces, it is clear that a sphere attached to an AFM tip can result in significantly different measured forces when scanning over various surface regions. One should perhaps also mention that while gold systems also suffer from patch potential problems there are experimental methods used to work around that. Our key message is that differences in predicted sphere-surface separation are not only due to surface roughness or different electrostatic interactions but also partly due to heterogeneous surface patches. In the case of gapped metal systems, these patches can spontaneously form during surface manufacturing.

ACKNOWLEDGMENTS

M.B., S.P., and O.I.M.'s research contributions are part of the Project No. 2022/47/P/ST3/01236 cofunded by the National Science Centre and the European Union's Horizon 2020 research and innovation programme under the Marie Skłodowska-Curie Grant Agreement No. 945339. The research by M.B. and S.P. took place at the "ENSEMBLE3 - Centre of Excellence for nanophotonics, advanced materials and novel crystal growth-based technologies" Project (Grant Agreement No. MAB/2020/14) carried out within the International Research Agendas programme of the Foundation for Polish Science cofinanced by the European Union under the European Regional Development Fund, the European Union's Horizon 2020 research and innovation programme Teaming for Excellence (Grant Agreement. No. 857543) for support of this work. S.O. thanks the National Science Centre, Poland (Grant No. UMO/2020/39/I/ST4/01446) and the "Excellence Initiative - Research University" (IDUB) Program, Action I.3.3 - "Establishment of the Institute for Advanced Studies (IAS)" for funding (Grant No. UW/IDUB/2020/25). We gratefully acknowledge Poland's high-performance computing infrastructure PLGrid (HPC Centers: ACK Cyfronet AGH) for providing computer facilities and support within computational Grant No. PLG/2023/016228 and for awarding this project access to the LUMI supercomputer, owned by the EuroHPC Joint Undertaking, hosted by CSC (Finland) and the LUMI consortium through Grant No. PLL/2023/4/016319.

TABLE II. The fitting function for silica–air–gapped metal surface is $y = x^{a\,\log(x)}\, x^b\, e^c$ with a, b, and c are unitless parameters given in the table.

Material	a	b	c
$BaNbO_3$	−0.006247	−0.55217	−2.993454
$Ba_{0.88}NbO_3$	−0.006368	−0.554738	−3.033964
$Ba_{0.6}NbO_3$	−0.006260	−0.552784	−3.005466
$BaNb_{0.86}O_3$	−0.006389	−0.554454	−3.029188
$Ba_{0.5}NbO_3$	−0.006898	−0.562608	−3.093622
$Ca_6Al_7O_{16}$	−0.005989	−0.554364	−3.184238
$Ca_{5.75}Al_7O_{16}$	−0.006070	−0.555309	−3.203518
$Ca_{5.5}Al_7O_{16}$	−0.007034	−0.569185	−3.297207

APPENDIX A: FITTING FUNCTIONS AND THEIR ANALYSIS

Here, we discuss the fitting curve and parameters for distance vs Casimir-Lifshitz force plot between different material combinations of $Ba_{1-x}Nb_{1-y}O_3$ and $Ca_{6-x}Al_7O_{16}$ with silica (SiO_2) and gold (Au) sphere where the intermediate medium is air. We provide Tables II and III for the above combinations

TABLE III. The fitting function for gold–air–gapped metal surface is $y = x^{a\,\log(x)}\, x^b\, e^c$ with a, b, and c are unitless parameters given in the table.

Material	a	b	c
$BaNbO_3$	−0.004965	−0.522436	−2.294606
$Ba_{0.88}NbO_3$	−0.005023	−0.523520	−2.307484
$Ba_{0.6}NbO_3$	−0.005355	−0.528101	−2.344180
$BaNb_{0.86}O_3$	−0.005421	−0.528405	−2.342667
$Ba_{0.5}NbO_3$	−0.006139	−0.538088	−2.410562
$Ca_6Al_7O_{16}$	−0.005075	−0.529580	−2.498146
$Ca_{5.75}Al_7O_{16}$	−0.005267	−0.531884	−2.523991
$Ca_{5.5}Al_7O_{16}$	−0.006356	−0.545063	−2.614540

TABLE IV. Parametrization of the average dielectric function of continuous media, $\varepsilon(i\xi)$, at imaginary frequencies for $Ca_{6-x}Al_7O_{16}$ as calculated with first-principles calculations and a damping coefficient (Γ) set to 0.2 eV. The ω_j modes are given in eV. The largest difference between fitted and calculated $\varepsilon(i\xi)$ is 0.08%.

	Coefficients (C_j) for different $Ca_{6-x}Al_7O_{16}$ compounds		
Modes (ω_j)	$Ca_6Al_7O_{16}$	$Ca_{5.75}Al_7O_{16}$	$Ca_{5.5}Al_7O_{16}$
0.0206	58.9601	0.6494	0.0001
0.0347	91.1774	1.797	0.0003
0.0587	57.4068	5.2997	0.001
0.1013	16.4729	15.4951	0.0221
0.1996	73.0451	29.8463	0.3283
0.3938	0.3949	2.1519	0.7511
0.9556	0.0706	0.2519	0.4345
2.2773	0.0987	0.0392	0.0
6.4732	0.4594	0.2384	0.2279
10.2048	0.7938	0.8189	0.0
18.2421	0.3705	0.474	0.0486
30.9018	0.1655	0.2388	0.0
54.455	0.0059	0.0283	0.001

for the fitted unitless parameters a, b, and c. These parameters are used to illustrate surface variance Δd as a function of d_s in Figs. 6(a) and 6(b). These data give us some information on insulating and metallic surface patches for different stoichiometries.

APPENDIX B: PARAMETERISED DIELECTRIC FUNCTIONS OF THE GAPPED METALS

In order to link optical calculations from DFT with force calculations, we parameterized the dielectric functions for the different gapped metals used in Tables IV and V.

TABLE V. Parametrization of the average dielectric function of continuous media $\varepsilon(i\xi)$ at imaginary frequencies for $Ba_{1-x}Nb_{1-y}O_3$ as calculated with first-principles calculations and a damping coefficient (Γ) set to 0.2 eV. The ω_j modes are given in eV. The largest difference between fitted and calculated $\varepsilon(i\xi)$ is 0.1%.

Modes (ω_j)	Coefficients (C_j) for different $Ba_{1-x}Nb_{1-y}O_3$ compounds				
	$BaNbO_3$	$BaNb_{0.88}O_3$	$Ba_{0.6}NbO_3$	$BaNb_{0.86}O_3$	$Ba_{0.5}NbO_3$
0.0215	9.4105	69.1791	10.1195	0.6139	0.0
0.0438	17.6756	94.1209	15.8813	4.5368	0.0
0.0872	19.2732	66.833	17.5738	7.3998	0.0
0.1967	451.2032	351.9936	83.8965	80.6752	0.0
0.2227	53.9568	37.1564	35.407	0.0	0.0
0.6448	0.2725	1.3619	1.6775	6.027	0.0
2.5296	0.1729	0.1616	0.3952	0.6325	0.2161
5.0772	1.2805	1.5587	2.4751	1.2681	2.4029
8.4405	1.5742	1.3843	0.8565	1.7721	1.0033
16.0637	0.7289	0.7517	0.8088	0.5311	0.717
27.1476	0.2407	0.2107	0.1615	0.3452	0.1712
47.1511	0.0632	0.0695	0.0824	0.0074	0.0782
79.6918	0.0029	0.0	0.0	0.0114	0.0

[1] H. B. G. Casimir, On the attraction between two perfectly conducting plates, K. Ned. Akad. Wet. **51**, 793 (1948).

[2] I. E. Dzyaloshinskii, E. M. Lifshitz, and L. P. Pitaevskii, The general theory of van der Waals forces, Adv. Phys. **10**, 165 (1961).

[3] B. E. Sernelius, *Fundamentals of van der Waals and Casimir Interactions*, Springer Series on Atomic, Optical, and Plasma Physics (Springer International Publishing, Switzerland, 2018).

[4] G. L. Klimchitskaya and V. M. Mostepanenko, Casimir effect invalidates the Drude model for transverse electric evanescent waves, Physics **5**, 952 (2023).

[5] M. Boström, M. R. Khan, H. R. Gopidi, I. Brevik, Y. Li, C. Persson, and O. I. Malyi, Tuning the Casimir-Lifshitz force with gapped metals, Phys. Rev. B **108**, 165306 (2023).

[6] A. G. Grushin and A. Cortijo, Tunable Casimir repulsion with three-dimensional topological insulators, Phys. Rev. Lett. **106**, 020403 (2011).

[7] D. A. T. Somers, J. L. Garrett, K. J. Palm, and J. N. Munday, Measurement of the Casimir torque, Nature (London) **564**, 386 (2018).

[8] G. H. Nyland and I. Brevik, Van der Waals interaction between two cylinders in a magnetic fluid, Physica A **202**, 81 (1994).

[9] S. K. Lamoreaux, Demonstration of the Casimir force in the 0.6 to 6 μm range, Phys. Rev. Lett. **78**, 5 (1997).

[10] A. O. Sushkov, W. J. Kim, D. A. R. Dalvit, and S. K. Lamoreaux, Observation of the thermal Casimir force, Nat. Phys. **7**, 230 (2011).

[11] W. Ducker, T. Senden, and R. Pashley, Direct measurement of colloidal forces using an atomic force microscope, Nature (London) **353**, 239 (1991).

[12] A. Zunger and O. I. Malyi, Understanding doping of quantum materials, Chem. Rev. **121**, 3031 (2021).

[13] O. I. Malyi, M. T. Yeung, K. R. Poeppelmeier, C. Persson, and A. Zunger, Spontaneous non-stoichiometry and ordering in degenerate but gapped transparent conductors, Matter **1**, 280 (2019).

[14] O. I. Malyi and A. Zunger, False metals, real insulators, and degenerate gapped metals, Appl. Phys. Rev. **7**, 041310 (2020).

[15] W. Broer, G. Palasantzas, J. Knoester, and V. B. Svetovoy, Roughness correction to the Casimir force at short separations: Contact distance and extreme value statistics, Phys. Rev. B **85**, 155410 (2012).

[16] J. P. Perdew, K. Burke, and M. Ernzerhof, Generalized gradient approximation made simple, Phys. Rev. Lett. **77**, 3865 (1996).

[17] S. L. Dudarev, G. A. Botton, S. Y. Savrasov, C. J. Humphreys, and A. P. Sutton, Electron-energy-loss spectra and the structural stability of nickel oxide: An LSDA+U study, Phys. Rev. B **57**, 1505 (1998).

[18] G. Kresse and J. Hafner, *Ab Initio* molecular dynamics for liquid metals, Phys. Rev. B **47**, 558 (1993).

[19] G. Kresse and J. Furthmüller, Efficiency of *ab-initio* total energy calculations for metals and semiconductors using a plane-wave basis set, Comput. Mater. Sci. **6**, 15 (1996).

[20] G. Kresse and J. Furthmüller, Efficient iterative schemes for *ab initio* total-energy calculations using a plane-wave basis set, Phys. Rev. B **54**, 11169 (1996).

[21] G. Kresse and D. Joubert, From ultrasoft pseudopotentials to the projector augmented-wave method, Phys. Rev. B **59**, 1758 (1999).

[22] L. D. Landau and E. M. Lifshitz, *Statistical Physics, Part 1*, 3rd ed. (Elsevier, Amsterdam, 2013), Vol. 5.

[23] P. Blaha, K. Schwarz, F. Tran, R. Laskowski, G. K. H. Madsen, and L. D. Marks, WIEN2k: An APW+ lo program for calculating the properties of solids, J. Chem. Phys. **152**, 074101 (2020).

[24] P. Blaha, K. Schwarz, P. Sorantin, and S. B. Trickey, Full-potential, linearized augmented plane wave programs for crystalline systems, Comput. Phys. Commun. **59**, 399 (1990).

[25] O. I. Malyi, M. Boström, V. V. Kulish, P. Thiyam, D. F. Parsons, and C. Persson, Volume dependence of the dielectric properties of amorphous SiO_2, Phys. Chem. Chem. Phys. **18**, 7483 (2016).

[26] M. Boström, O. I. Malyi, P. Parashar, K. V. Shajesh, P. Thiyam, K. A. Milton, C. Persson, D. F. Parsons, and I. Brevik, Lifshitz interaction can promote ice growth at water-silica interfaces, Phys. Rev. B **95**, 155422 (2017).

[27] Y. Li, K. A. Milton, I. Brevik, O. I. Malyi, P. Thiyam, C. Persson, D. F. Parsons, and M. Boström, Premelting and formation of ice due to Casimir-Lifshitz interactions: Impact of improved parameterization for materials, Phys. Rev. B **105**, 014203 (2022).

[28] Z. Babamahdi, V. B. Svetovoy, M. Enache, M. Stöhr, and G. Palasantzas, Comparison of Casimir forces and electrostatics from conductive SiC-Si/C and Ru surfaces, Phys. Rev. B **100**, 245422 (2019).